ARTICLE

A mixed valence diruthenium (II, III) complex endowed with high stability: from experimental evidences to theoretical interpretation

Received 00th January 20xx,
Accepted 00th January 20xx

DOI: 10.1039/x0xx00000x

Elisabetta Barresi,[†a] Iogann Tolbatov,[†b] Alessandro Pratesi,[c] Valentina Notarstefano,[d] Emma Baglini,[a] Simona Daniele,[a,e] Sabrina Taliani,[a,e] Nazzareno Re,*[b] Elisabetta Giorgini,*[d] Claudia Martini,[a,e] Federico Da Settimo,[a,e] Tiziano Marzo *[a,e] and Diego La Mendola[a]

We report here on the synthesis and multi-technique characterization of [Ru_2Cl((2-phenylindol-3-yl)glyoxyl-L-leucine-L-phenylalanine)$_4$] a novel diruthenium (II,III) complex obtained reacting [$Ru_2(\mu\text{-}O_2CCH_3)_4Cl$] with a dual indolylglyoxylyl dipeptide anticancer agent. We soon realised that the compound is very stable in several different conditions including aqueous buffers or organic solvents. It is also completely unreactive toward proteins. The high stability is also suggested by cellular experiments in a glioblastoma cell line. Indeed, while the ligand exerts high cytotoxic effects in the low μM range, the complex is completely non-cytotoxic against the same line, most probably because of the lack of ligand release. To investigate the reasons of such high stability, we carried out DFT calculations that are fully consistent with the experimental findings. Results highlight that the stability of [Ru_2Cl((2-phenylindol-3-yl)glyoxyl-L-leucine-L-phenylalanine)$_4$] relies on the nature of the ligand, including its steric hindrance that prevents the reaction of any nucleophilic group with the Ru_2 core. The ligand displacement is the key step to allow the reactivity with biological targets of metal-based prodrugs. Accordingly, we discuss the implications of some important aspects that should be considered when active molecules are chosen as ligand for the synthesis of paddle-wheels like complexes with medicinal applications.

Introduction

Forty years after its approval by FDA, cisplatin remains among the most used molecules in the treatment of cancer patients.[1–3] Though it is effective to fight several kinds of tumour, resistance phenomena and heavy side effects may represent limiting aspects leading to treatment failure.[4,5] To overcome these problems many cisplatin-inspired platinum drugs with various ligands have been synthesised and explored for their anticancer activity and some of them i.e. oxaliplatin and carboplatin have been approved and to date are widely used in clinical practice worldwide.[6–8] Also, in the last decades, a few platinum-based antineoplastic agents have received local approval. This is the case of nedaplatin, heptaplatin and lobaplatin that entered the clinic in Japan, Korea and China respectively.[6,8]

Owing to the wide versatility of transition metals many non-platinum complexes have been also developed and tested.[9–11] The use of metals different from platinum is attractive because various oxidation states, hard/soft properties, stability and coordination geometries as well as thermodynamic and kinetic features can be conveniently exploited to selectively bind biological targets triggering specific cell responses and the desired pharmacological effects.[8,12–14]

Some notable results were obtained for a few ruthenium (II) and (III) compounds. Among several, NAMI-A and KP1019/KP1339 reached clinical trials for their promising properties as antimetastatic and cytotoxic agents respectively.[15,16] The positive outcome from these ruthenium compounds further fueled the attention on this transition metal.[17–19] A very attractive category of Ru-based compounds is that of diruthenium complexes bearing a direct metal-metal bond and a typical (II,III) mixed valence (Figure 1).

[a] Department of Pharmacy, University of Pisa. Via Bonanno Pisano, 6, 56126, Pisa, Italy. E-mail: tiziano.marzo@unipi.it
[b] Dipartimento di Farmacia, Università degli Studi "G. D'Annunzio" Chieti-Pescara, Via dei Vestini, I-66100 Chieti, Italy. E-mail: nre@unich.it
[c] Department of Chemistry and Industrial Chemistry, University of Pisa, Via G. Moruzzi, 13, 56124 Pisa, Italy.
[d] Department of Life and Environmental Sciences, DiSVA, Università Politecnica delle Marche, Via Brecce Bianche, 60131, Ancona, Italy. E-mail: e.giorgini@staff.univpm.it
[e] CISUP-Centro per l'Integrazione della Strumentazione Scientifica dell'Università di Pisa, University of Pisa, Italy

† These authors equally contributed.
Electronic Supplementary Information (ESI) available: UV-Vis and HR ESI-MS spectra with experimental and theoretical isotope pattern, and details for interaction with proteins, calculated bond distances for $[Ru_2(\mu\text{-}O_2CCH_3)_4Cl_2]^-$, Cartesian coordinates of the optimized complexes $[Ru_2(\mu\text{-}O_2CCH_3)_4Cl]$, $[Ru_2(EB106)_4Cl]$, and $[Ru_2(\mu\text{-}O_2CCH_3)_4(H_2O)_2]^+$. See DOI: 10.1039/x0xx00000x

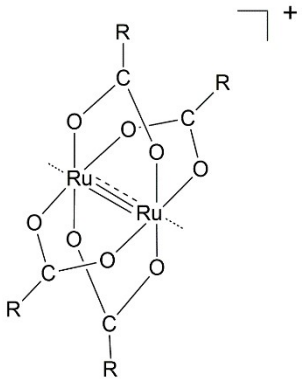

Fig. 1 General chemical structure of paddle-wheel Ru_2 (II, III) complexes.

The presence of three unpaired electrons delocalized on antibonding metal-metal orbitals, formally imparts a charge of +2.5 to each ruthenium atom.[20] The parent complex of Ru_2 (II,III) compounds is $[Ru_2(\mu\text{-}O_2CCH_3)_4Cl]$ namely (acetato)chloridodiruthenium (II,III), that was synthesized and characterized for the first time by Wilkinson and Stephenson.[21] It has been widely investigated in the past and the crystal structure was solved for the first time in 1969 by Cotton and coworkers.[21,22] In the solid state the two axial positions are occupied by chloride ligands that are responsible for bridging each other the bimetallic cores forming the typical polymeric structure. The polymeric structure can be broken in solution by the axial coordination of solvent molecules leading to the $[Ru_2(RCOO)_4L_2]^n$, where L is a neutral solvent molecule or an anionic ligand and n = −1, 0 or +1. Also, Ru_2 mixed valence complexes possess unique physical and chemical properties making them widely exploited for several applications in material science, magnetic materials, catalysis, synthesis of other paddle-wheel compounds as well as in medicine.[20,23]

Recently, some of us obtained interesting results by reacting $[Ru_2(\mu\text{-}O_2CCH_3)_4Cl]$ in presence of the model protein lysozyme. Upon incubation, an adduct was formed where two out four acetate ligands were displaced by two water molecules and an aspartate residue of the protein. Thus, the stable lysozyme-$[Ru_2(\mu\text{-}O_2CCH_3)_2(H_2O)_2]^{3+}$ was obtained and characterized through high resolution ESI-MS and X-ray crystallography.[24] Next, considering the catalytic properties of the Ru_2 (II,III) center[25,26] the isolated diruthenium–HEWL derivative (where HEWL is Hen Egg White Lysozyme) was investigated for its catalytic properties in the preparation of nitrones by means of aerobic oxidation of *N*,*N*-disubstituted hydroxylamines. Remarkably, when compared with $[Ru_2(\mu\text{-}O_2CCH_3)_4Cl]$, the diruthenium–HEWL derivative, was not only found to preserve the catalytic features, but it was also capable to confer a complete chemoselectivity to the reaction, thus enhancing the catalytic properties of $[Ru_2(\mu\text{-}O_2CCH_3)_4Cl]$ and delineating diruthenium–HEWL as an artificial metalloenzyme.[27]

For medicinal purposes, $[Ru_2(\mu\text{-}O_2CCH_3)_4Cl]$ can be used as starting material for the obtainment of analogues bearing different pharmacologically active ligands in place of the acetate ones. This strategy is fascinating because associates the medicinal properties of ruthenium centers with the activity of the R-COO^- drug that acts as bidentate ligand through the carboxylic group. Moreover, any molecule of complex contains four active ligands that can be delivered. In this frame, de Oliveira Silva and coworkers have reported several Ru_2 (II,III) compounds prepared from $[Ru_2(\mu\text{-}O_2CCH_3)_4Cl]$. Specifically, in their papers the acetate ligands were replaced by non-steroidal antinflammatory agents including naproxen and ibuprofen and tested against various cancer cell lines with some appreciable result. In fact, complex bearing four ibuprofen molecules was found active against glioma tumor models and effective in reducing gastric ulceration in *in vivo* models.[28,29]

On the ground of these premises we recently started to consider the chance to synthesize a novel Ru_2 (II,III) derivative where the four molecules coordinating the Ru_2 core were the indolylglyoxylyldipeptide compound (EB106 hereafter) rationally designed as dually-active agent capable of simultaneous activation of TSPO and p53 (Figure 2).

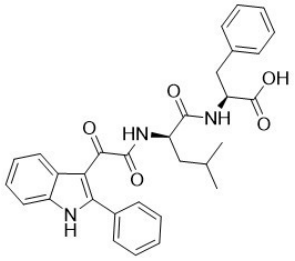

Fig. 2 Chemical structure of EB106.

EB106 was previously synthesized and characterized for its biological effects *in vitro* in a glioblastoma multiforme model (GBM). The compound is able to bind TSPO and the MDM2 (Murine Double Minute 2) protein, the most relevant physiological inhibitor of p53, thus restoring its activity in a functional manner. This causes the mitochondrial permeability transition pore opening, eventually leading to transmembrane mitochondrial potential dissipation. In GBM model, EB106 induces a potent effect resulting in the inhibition of cell viability in the low µM range as result of the concomitant activation of TSPO and p53.[30]

The novel complex $[Ru_2(EB106)_4Cl]$ was obtained and fully characterized through independent chemico-physical methods. Quite soon we realized that it was very stable both in organic solvents and physiological-like conditions. At variance with the parent drugs, $[Ru_2(\mu\text{-}O_2CCH_3)_4Cl]$ it was unreactive toward protein targets and non-cytotoxic in a representative glioblastoma cell line where EB106 exerted a potent cytotoxic effect. Spurred by these experimental evidences we have theoretically investigated the reasons for such stability. Some notable results emerged and are here comprehensively analyzed and discussed. Importantly, the overall evaluation of our findings indicates that the chemical nature of the Ru_2 bound active ligands may have a dramatic impact into the activation profile of the complex, and in specific cases, may result in a complete inactivation of the pharmacological properties of the ligand itself. Thus, relevant aspects to be considered in the choice of the ligands for the Ru (II, III) core are delineated.

Experimental

All the chemicals were used without further purification. [$Ru_2(\mu\text{-}O_2CCH_3)_4Cl$] was synthesised following the reported procedure.[24] 2-phenylindol-3-yl)glyoxyl-L-leucine-L-phenylalanine (EB106) was synthesised as previously described.[30]

Synthesis of [$Ru_2(EB106)_4Cl$]

Synthesis of [$Ru_2(EB106)_4Cl$] was performed with a slight modification of the reported procedures.[20,31] Briefly, in a 100 mL flask, 50 mg (0.1 mol) of [$Ru_2(\mu\text{-}O_2CCH_3)_4Cl$] were solubilised in hot water (10 mL). Next, 273 mg (0.5 mol) of EB106 were solubilised in ethanol (10 mL) and added dropwise to the water solution of [$Ru_2(\mu\text{-}O_2CCH_3)_4Cl$]. The mixture was refluxed under vigorous magnetic stirring for 24 h. A sticky black product was obtained very soon (within few minutes). After 24 h the mixture was cooled to room temperature and rapidly decanted. 20 mL of a fresh water/ethanol mixture (1 : 1) were added again to the black product formed. Then, reflux was allowed for further 5 h. After this time, the reflux was stopped and the mixture filtered immediately. On cooling, the black product that turned solid/crystalline from sticky, was extensively washed with 1 : 1 mixture ethanol : water and diethyl ether. Finally, the obtained compound was dried under reduced pressure and characterized through elemental analysis (EA), high-resolution mass spectrometry and IR spectroscopy. Yield: 37 %. EA [Ru_2Cl((2-phenylindol-3-yl)glyoxyl-L-leucine-L-phenylalanine)$_4$].
Calculated for $C_{124}H_{120}ClN_{12}O_{20}Ru_2 \cdot 12\ H_2O$: C = 58.36; H = 5.69; N = 6.59. Experimental: C = 58.08; H = 5.43; N = 6.45. HR-ESI-MS: [Ru_2Cl((2-phenylindol-3-yl)glyoxyl-L-leucine-L-phenylalanine)$_4$] *m/z* $[M\text{-}Cl]^+$ = 2300.68256 (theoretical: 2300.68233; error: 0.1 ppm, see supporting material for further details). IR (ν_{max}/cm^{-1}): 3063 and 3033 ν (C–H aromatic); 2959 and 2870 ν (C-H aliphatic); 1666br ν (C=O); 1525 coupling of δ (N-H) and ν (C-N); 1452 δ (C-H); 1429 ν (C-N); 1194 ν (C-O); 751 δ (C-H aromatic), and 699 δ (O-C-O).

HR-ESI-MS characterization

[$Ru_2(EB106)_4Cl$] was dissolved in LC-MS grade ethanol to a final concentration of 10^{-5} M and the high-resolution ESI mass spectrum was recorded on this solution with 0.1 % v/v of formic acid added just before the analysis. The spectrum was recorded in positive polarity by direct injection at a 5 µL min^{-1} flow rate in a TripleTOF® 5600+ high-resolution mass spectrometer (Sciex, Framingham, MA, USA), equipped with a DuoSpray® interface operating with an ESI probe. The ESI source parameters were optimized and were as follows: Ionspray Voltage Floating 5500 V, Temperature 37 °C, Ion source Gas 1 (GS1) 30; Ion source Gas 2 (GS2) 0; Curtain Gas (CUR) 20, Declustering Potential (DP) 100 V, Collision Energy (CE) 10 V. For acquisition, Analyst TF software 1.7.1 (Sciex) was used and the spectra was elaborated with PeakViewTM software v.2.2 (Sciex).

Solution behaviour and interaction with protein

The solution behaviour of [$Ru_2(EB106)_4Cl$] as well as protein interaction studies were performed through spectrophotometric analysis using a Varian Cary 50 Bio UV-Vis spectrophotometer.[24,32] The spectral profiles were recorded for 72 h. Firstly, it was ascertained the stability of compound in organic solvents: DMSO, MeOH, EtOH, DMF. To assess [$Ru_2(EB106)_4Cl$] solution behavior at physiological-like pH, a stock solution of compound was prepared and added to a 10 mM phosphate buffer to a final concentration of 10^{-5} M in presence of 40 % of DMSO. Protein interaction studies were conducted in the same buffer in presence of 15 % of DMSO with an excess of [$Ru_2(EB106)_4Cl$] (complex to protein ratio 3 : 1).[32] The absorbance was monitored in the range between 250 and 800 nm at 25 °C. ESI-MS spectra were also recorded to study the interaction of [$Ru_2(EB106)_4Cl$] with proteins (See SI for experimental details) following a well-established protocol already used in our lab.[32]

IR spectroscopy

The IR measurements of EB106, [$Ru_2(EB106)_4Cl$] and [$Ru_2(\mu\text{-}O_2CCH_3)_4Cl$] were performed using an INVENIO FTIR Spectrometer (Bruker Optics, Ettlingen, Germany), coupled with a Platinum ATR (Attenuated Total Reflectance) accessory for the analysis of solid samples in reflectance mode and equipped with a DTGS (Deuterated Triglycine Sulphate) detector. For each compound, 5 spectra were acquired in the 4000-400 cm^{-1} spectral range (128 scans, spectral resolution 4 cm^{-1}). Before each sample measurement, a background spectrum was acquired in the same experimental conditions on the clean diamond crystal. Raw IR spectra were then submitted to absorbance conversion, polynomial baseline correction (64 baseline points) and vector normalization (OPUS 7.5, Bruker Optics, Ettlingen, Germany). Finally, for each compound, the average spectrum was calculated.

Cell culture and proliferation assay

U87MG cells were maintained in RPMI medium supplemented with 10 % FBS, 2 mM-glutamine, 100 U/ml penicillin, 100 mg/ml streptomycin and 1 % nonessential amino acids at 37 °C in 5 % CO_2.[33] The cells were plated at 5 x 10^3 cells/cm^2. After 24 h, U87MG cells were challenged with fresh medium containing the tested compounds, EB106 and [$Ru_2(EB106)_4Cl$].[30,33] Following incubation, cell proliferation was investigated by MTS assay according to manufacturer's instruction. The absorbance of formazan at 490 nm was read in a colorimetric assay with an automated plate reader.[34] The nonlinear multipurpose curve-fitting program Graph-Pad Prism (GraphPad Software Inc., San Diego, CA) was used for data analysis and graphic presentations. The data are presented as the mean ± SEM.

Theoretical calculations

Calculations on $[Ru_2(\mu\text{-}O_2CCH_3)_4L_2]$ and $[Ru_2(\mu\text{-}O_2CCH_3)_3$ (EB106)$L_2]$ model complexes were performed with density functional theory (DFT) using the B3LYP hybrid functional[35,36] which is known to give a good description of geometries and reaction profiles for transition-metal-containing compounds[37–39] and employing the Jaguar 9.1[40] quantum chemistry package. Optimizations were carried out in gas phase with the LACVP**basis set of polarized double-ζ quality.[41]Single point electronic energy calculations were performed on the gas-phase geometries with the triple-ζ quality basis set 6-311++G** and the ECP LACV3P**++. Cartesian coordinates of optimized complexes $[Ru_2(\mu\text{-}O_2CCH_3)_4Cl]$, $[Ru_2(EB106)_4Cl]$, and $[Ru_2(\mu\text{-}O_2CCH_3)_4(H_2O)_2]^+$ are included in Supporting Information.

Frequency calculations were performed to verify the correct nature of the stationary points and to estimate zero-point energy (ZPE) and thermal corrections to thermodynamic properties. The Poisson–Boltzmann (PB) continuum solvent method was used to describe the solvation.[42] Solvation energies were calculated on gas-phase stationary points with the same basis set employed for single point calculations.

Calculations on the $[(H_2O)Ru_2(EB106)_4(H_2O)]^+$ complex have been performed with the hybrid QM/MM approach which is known to provide the accurate geometries for large molecules with transition metal centers,[43,44] using the Qsite 5.8 software package.[45] The QM region included 2 ruthenium atoms, 2 water molecules, and the first 8 non-H atoms with all H atoms bonded to them on each EB106 tail (4 tails were included) and was treated at DFT level of theory with the LACVP** basis set and the B3LYP functional, whereas the MM system consisting of the remaining protein atoms was described with the OPLSA_2001 force field.[46]

The surfaces featured in Figure 6 were produced by means of Maestro (Schrödinger Release 2020-2: Maestro, Schrödinger, LLC, New York, NY, 2020). The solvent-accessible surfaces were calculated for the acetone solvent (its probe radius was calculated to be 2.44 A by Maestro). The van der Waals surfaces have been calculated with the exclusion of the carboxylate oxygens.

Results and discussion

Synthesis, characterization and solution chemistry of $[Ru_2(EB106)_4Cl]$

The synthesis of the compound was performed as reported in the experimental section. The characterization was straightforwardly carried out through a multi-technique approach including ESI-MS and IR spectroscopy. The ESI mass spectrum (Fig. 3) confirms the obtainment of the compound being the signal at 2300.68256 *m/z* assignable to the monocationic fragment $[Ru_2(EB106)_4]^+$.

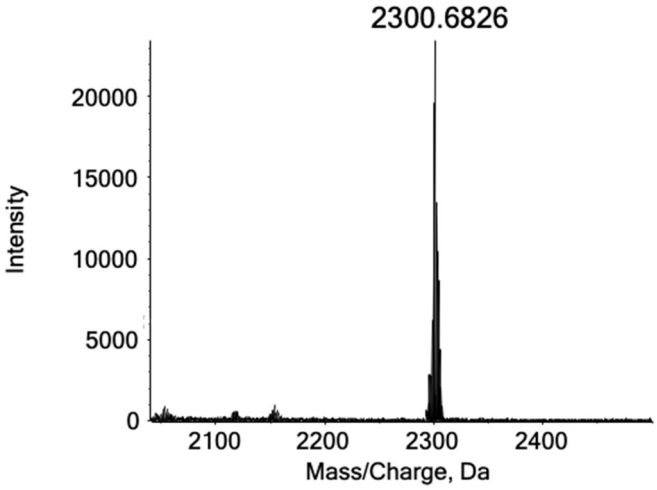

Fig. 3 High-resolution ESI mass spectrum of $[Ru_2(EB106)_4Cl]$, 10^{-5} M, EtOH.

A further confirmation is provided by the comparison of the IR spectra recorded on EB106, $[Ru_2(EB106)_4Cl]$ and $[Ru_2(\mu\text{-}O_2CCH_3)_4Cl]$, considered as parent complex (Fig. 4). The comparative inspection of the IR spectral profiles of EB106 and $[Ru_2(EB106)_4Cl]$ is indicative of complex formation. In fact, in the $[Ru_2(EB106)_4Cl]$ IR spectrum, all the bands attributable to EB106, were found, with the only exception of the band centered at 1730 cm^{-1}, assigned to the C=O stretching of the carboxylic group. The lack of this band strongly indicates the occurrence of a coordination between EB106 and the Ru_2 core. Moreover, a different spectral profile was found between $[Ru_2(EB106)_4Cl]$ and $[Ru_2(\mu\text{-}O_2CCH_3)_4Cl]$, which only shared the bands at: 2959 cm^{-1} and 2870 cm^{-1} (assigned to the stretching of aliphatic C-H and shifted in $[Ru_2(\mu\text{-}O_2CCH_3)_4Cl]$ at 2940 cm^{-1} and 2850 cm^{-1}, respectively) 1452 cm^{-1} (assigned to the bending of aliphatic C-H), and 699 cm^{-1} (assigned to the bending of O-C-O).[47]

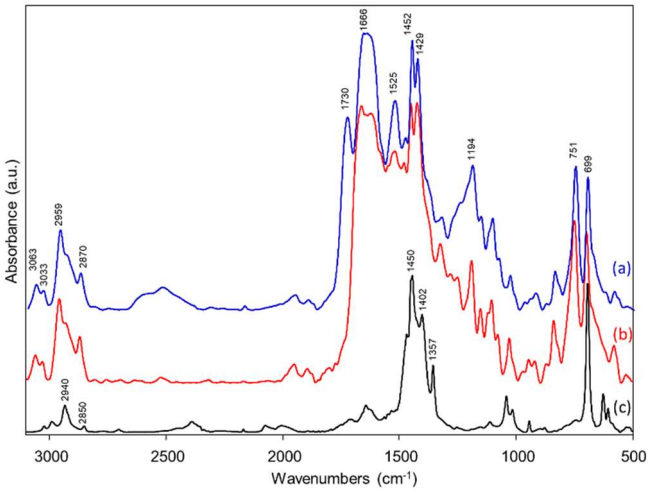

Fig. 4 IR spectra of (**a**) EB106, (**b**) $[Ru_2(EB106)_4Cl]$ and (**c**) $[Ru_2(\mu\text{-}O_2CCH_3)_4Cl]$.

Next, we explored the solution behaviour of the complex spectrophotometrically. It is soluble and very stable in DMSO as well as in ethanol and methanol or DMF even for long incubation times. Similarly, it is stable in presence of aqueous phosphate buffer at physiological-like pH (Fig. 5).

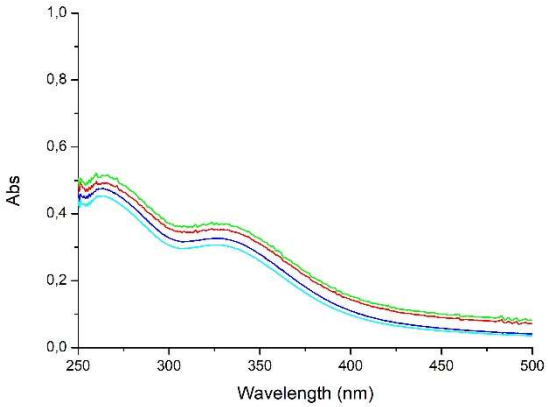

Fig. 5 Time dependent UV-Vis analysis of $[Ru_2(EB106)_4Cl]$, 10^{-5} M in 10 mM phosphate buffer in presence of 40 % DMSO (pH = 7.4) followed for 72 h.

In this latter case we used 40 % of DMSO to avoid precipitation of the complex. Despite of this, the slight drift of the baseline indicates the occurrence of precipitation. However, over 72 h the shape of the two bands falling at about 260 and 340 nm and assignable to $\pi \rightarrow \pi^*$ electronic transitions of the peptide bonds and aromatic moieties, remained unaltered and no new bands appeared in the range 250-800 nm.[48] Worth to mention, also the charge-transfer σ (axial ligand) $\rightarrow \sigma^*(Ru_2)$ transition bands could fall in the range 340-350 nm thus determining possible overlaps.[49] Altogether, these UV-Vis evidences point out the stability of the complex also in these experimental conditions.

Protein interaction studies

To shed light on the likely mechanisms of activation of $[Ru_2(EB106)_4Cl]$, we performed bioinorganic studies to assess the reactivity in presence of protein targets. [8,50–53]

It is worth reminding that the parent complex $[Ru_2(\mu\text{-}O_2CCH_3)_4Cl]$ reacts quantitatively with the model protein lysozyme giving rise to a characteristic adduct where one acetate ligand is replaced by the Asp101 or Asp119 residues.[24] However, when $[Ru_2(EB106)_4Cl]$ was reacted with this model protein, no adducts formation occurred as observed with ESI-MS analysis. Thus, we hypothesized that $[Ru_2(EB106)_4Cl]$ could interact with a panel of different proteins bearing various exposed coordination sites namely histidine, methionine, aspartate, cysteine residues, well known for their ability of ruthenium coordination.[8] Therefore, further incubation experiments were performed with human ferritin, ubiquitin, carbonic anhydrase, holo transferrin, superoxide dismutase, human serum albumin and hemoglobin. However, in both UV-Vis spectrophotometric analysis and ESI-MS experiments, no changes in the bands shape or appearance of new bands nor mass peaks assignable to adducts formation were observed (see SI for UV-Vis spectra and ESI-MS experimental details).

Antiproliferative effects

$[Ru_2(EB106)_4Cl]$ was then tested in comparison with EB106 in a representative glioblastoma cell line (i.e, U87MG cells). EB106 was highly effective in reducing U87MG cell proliferation, with a calculated IC_{50} of 3.12 ± 0.36 μM, consistent with previous data.[30] In contrast, $[Ru_2(EB106)_4Cl]$ did not significantly affect glioblastoma cell proliferation when administered up to 100 μM. The overall interpretation of the data obtained -in particular the lack of reactivity toward representative proteins bearing solvent exposed aminoacidic residues capable of coordinate ruthenium as well as the inhibition of the cytotoxic effects compared with EB106- may supports the mechanistic interpretation that the high stability of $[Ru_2(EB106)_4Cl]$ doesn't allow ligand displacement and thus the release of the pharmacologically active fragments.

DFT calculations

In order to verify the above hypothesis, we used computational methods. Firstly, theoretical calculations were carried out to assess the thermodynamics of the substitution of an acetate ion in $[Ru_2(\mu\text{-}O_2CCH_3)_4L_2]$ by EB106 species, and to elucidate the different reactivity patterns observed for $[Ru_2(\mu\text{-}O_2CCH_3)_4Cl]$ and $[Ru_2(EB106)_4Cl]$. To evaluate the accuracy of the employed level of theory we first carried out geometry optimization of the parent complex $[Ru_2(\mu\text{-}O_2CCH_3)_4Cl]$, whose X-ray structure is well known.[54] We found a good agreement between calculated and experimental geometries, with Ru-O and Ru-Cl distances within 0.04 Å, Ru-Ru distance within 0.1 Å and bond angles within 3°, see Table S1. We also calculated the reaction free energy for the axial anation reaction of the $[Ru_2(\mu\text{-}O_2CCH_3)_4(H_2O)_2]^+$, the predominant species observed in solution, with Cl^-:

$$[Ru_2(\mu\text{-}O_2CCH_3)_4(H_2O)_2]^+ + Cl^- \rightarrow [Ru_2(\mu\text{-}O_2CCH_3)_4(H_2O)Cl] + H_2O$$

for which a reaction free energy of 1.6 kcal mol^{-1} has been observed,[55,56] obtaining a reaction free energy of 2.0 kcal mol^{-1} in excellent agreement with the experimental data.

We then investigated the substitution of one acetate of $[Ru_2(\mu\text{-}O_2CCH_3)_4(H_2O)_2]^+$ by the ionized carboxylate group of EB106, the first step in the expected process for the synthesis of $[Ru_2(EB106)_4Cl]$ in water solution, to evaluate the thermodynamic feasibility of this reaction. The results show a barely endothermic reaction, ΔH=2.8 kcal mol^{-1} with a slightly larger reaction free energy of 4.4 kcal mol^{-1}, probably due to the loss of entropy when EB106 binds to the Ru_2 metal core.

We finally optimized through a QM/MM approach the geometry of the $[Ru_2(EB106)_4Cl]^+$ complex obtaining the structure reported in Figure 6b. Such a structure suggests that the reason behind the high stability of $[Ru_2(EB106)_4Cl]$ could be due to the steric hindrance of the compact arrangement around the Ru_2 core of the four large EB106 ligands whose arms prevent the approach of any nucleophilic group to the Ru bound carboxylate oxygens. Indeed, two phenyl rings with high steric hindrance and two propyl groups surround the Ru atoms and the carboxylate oxygens bound to them preventing the approach to the metal center of incoming nucleophiles. To better show this effect, we calculated both the Van der Waals and the solvent-accessible surfaces for the acetone solvent (which has the same volume and form as an approaching carboxylate group), and compared them with the corresponding surfaces for the analogue tetraacetate complex, see figure 6. Both surfaces clearly show that, at variance with the smaller $[Ru_2(\mu\text{-}O_2CCH_3)_4Cl]$ complex, in the EB106 analogue the carboxylate oxygens are deeply buried into the molecular cavity formed by the scaffold of the four EB106 ligands making them hardly accessible to an attacking carboxylate group, especially if it comes from a more sterically demanding residue.

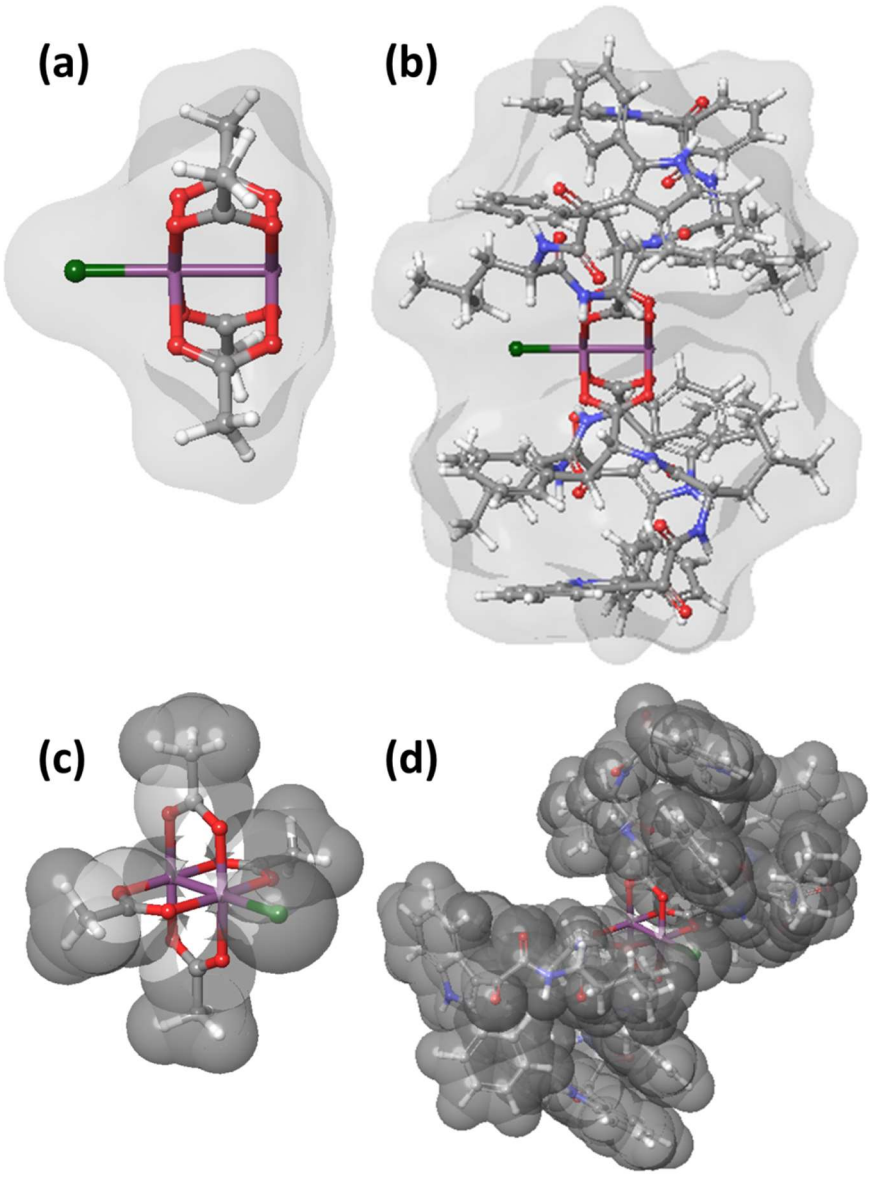

Fig. 6. The solvent-accessible surfaces of complexes $[(H_2O)Ru_2(\mu\text{-}O_2CCH_3)_4(H_2O)]$ (a) and $[(H_2O)Ru_2(EB106)_4(H_2O)]^+$ (b) and the corresponding van der Waals surfaces (c, d) produced with the exclusion of the carboxylate oxygens.

Overall, the newly synthesised compound $[Ru_2(EB106)_4Cl]$ was extensively characterized. The solution behavior of this novel complex was also studied pointing out its high stability both in presence of organic solvent and buffer at physiological pH. We observed that $[Ru_2(EB106)_4Cl]$, at variance of the parent complex bearing four acetate ligands[24], was unreactive when incubated with a representative panel of proteins. Indeed, from the results obtained through the multi-technique investigation strategy, no adducts formation nor ligands release were found. While these evidences clearly show the stability of the complex, a further confirmation came from the comparative analysis of the cytotoxic potency of EB106 and $[Ru_2(EB106)_4Cl]$ toward a glioblastoma cancer line. Experiments pointed out as $[Ru_2(EB106)_4Cl]$ is unable to induce anticancer effects even when administered at a 100 μM concentrations. Altogether, results suggest that the remarkable stability of $[Ru_2(EB106)_4Cl]$ is due to the nature of the EB106 ligand.

Conclusions

In this work we have reported the synthesis of a novel mixed valence (II, III) ruthenium complex i.e. $[Ru_2(EB106)_4Cl]$, where EB106 is the anticancer agent 2-phenylindol-3-yl)glyoxyl-L-leucine-L-phenylalanine. We designed $[Ru_2(EB106)_4Cl]$ to couple the interesting anticancer properties of EB106 with the medicinal properties of ruthenium core accompanied by the chance of multiple delivery of the active ligand.[15,16,28–30]. In contrast with the expectations, $[Ru_2(EB106)_4Cl]$ was unreactive toward protein targets and non-cytotoxic. We decided to investigate in more depth these features using an experimental and computational strategy. This approach allows to unveil as for ruthenium paddle-wheel shaped complexes the choice of the ligand with specific chemical properties is crucial and other aspects should be taken into account beyond the simple presence of the carboxylic group that is essential for the coordination to the Ru_2 (II,III) core. Indeed, if on one hand the use of these systems for medicinal applications may allow treatment improvement, on the other hand the nature of the ligand may have a dramatic impact on the overall chemical profile, impairing the activation process i.e. the ligand release (including the axial ones whose replacement is involved in the overall pharmacological activity)[57] and eventually the therapeutic effects. Our case is extremely instructive in this sense. In fact, it suggests that when approaching to the design of this family of prodrugs, one should carefully evaluate the chemical features of the active molecule to be coordinated to the Ru_2 core. Preferentially, molecules with a proper steric hindrance should be considered in order to avoid the impairment of the reactivity. Specifically, increasing the ligands occupancy, a decreased (or absent) reactivity/medicinal properties might be expected. In this frame computational methods can turn very indicative for the suitability of the selected ligand helping in predict the reactivity/accessibility of the bimetallic center, and indirectly may provide insights for the possible medicinal application. Noteworthy, if this balance is carefully evaluated some important advantages can be gained to optimize drug delivery and the desired pharmacological effects. Furthermore, the coordination to the Ru_2 core may allow to finely tune the stability of the synthesized compounds avoiding unwanted off-target reactions, thus improving the treatment itself.

Conflicts of interest

There are no conflicts to declare.

Acknowledgements

The authors thank Prof. Luigi Messori (Dept. of Chemistry "U. Schiff", University of Florence) for making available the TripleTOF® 5600+ mass spectrometer (Sciex, Framingham, MA, U.S.A.).

TM, DL and AP gratefully acknowledge the Beneficentia Stiftung, Vaduz (BEN2019/48, BEN2020/34 respectively) and University of Pisa (Rating Ateneo 2019-2020) for the financial support.

References

1 L. Kelland, *Nat. Rev. Cancer*, 2007, 7, 573–584.
2 D. Wang and S. J. Lippard, *Nat. Rev. Drug Discov.*, 2005, **4**, 307–320.
3 A. Macciò and C. Madeddu, *Expert Opin. Pharmacother.*, 2013, **14**, 1839–1857.
4 Y. Jung and S. J. Lippard, *Chem. Rev.*, 2007, **107**, 1387–1407.
5 S. Van Zutphen and J. Reedijk, *Coord. Chem. Rev.*, 2005, **249**, 2845–2853.
6 T. C. Johnstone, K. Suntharalingam and S. J. Lippard, *Chem. Rev.*, 2016, **116**, 3436–3486.
7 D. Cirri, S. Pillozzi, C. Gabbiani, J. Tricomi, G. Bartoli, M. Stefanini, E. Michelucci, A. Arcangeli, L. Messori and T. Marzo, *Dalt. Trans.*, **46**, 3311-3317.
8 T. Marzo, G. Ferraro, A. Merlino and L. Messori, in *Encyclopedia of Inorganic and Bioinorganic Chemistry*, Wiley, 2020, pp. 1–17.
9 N. P. E. Barry and P. J. Sadler, *Chem. Commun.*, 2013, **49**, 5106–5131.
10 I. Ott, *Coord. Chem. Rev.*, 2009, 253, 1670–1681.
11 E. Boros, P. J. Dyson and G. Gasser, *Chem*, 2020, **6**, 41–60.
12 K. Benjamin Garbutcheon-Singh, M. P. Grant, B. W. Harper, A. M. Krause-Heuer, M. Manohar, N. Orkey and J. R. Aldrich-Wright, *Curr. Top. Med. Chem.*, 2011, **11**, 521–542.
13 S. P. Fricker, in *Dalton Transactions*, Royal Society of Chemistry, 2007, pp. 4903–4917.
14 U. Jungwirth, C. R. Kowol, B. K. Keppler, C. G. Hartinger, W. Berger and P. Heffeter, *Antioxidants Redox Signal.*, 2011, **15**, 1085–1127.
15 C. G. Hartinger, S. Zorbas-Seifried, M. A. Jakupec, B. Kynast, H. Zorbas and B. K. Keppler, *J. Inorg. Biochem.*, 2006, **100**, 891–904.
16 E. Alessio, *Eur. J. Inorg. Chem.*, 2017, 2017, 1549–1560.

17 S. David, R. S. Perkins, F. R. Fronczek, S. Kasiri, S. S. Mandal and R. S. Srivastava, *J. Inorg. Biochem.*, 2012, **111**, 33–39.

18 L. Zeng, P. Gupta, Y. Chen, E. Wang, L. Ji, H. Chao and Z. S. Chen, *Chem. Soc. Rev.*, 2017, 46, 5771–5804.

19 A. Notaro and G. Gasser, *Chem. Soc. Rev.*, 2017, **46**, 7317–7337.

20 M. A. S. Aquino, *Coord. Chem. Rev.*, 1998, **170**, 141–202.

21 T. A. Stephenson and G. Wilkinson, *J. Inorg. Nucl. Chem.*, 1966, **28**, 2285–2291.

22 M. J. Bennett, K. G. Caulton and F. A. Cotton, *Inorg. Chem.*, 1969, **8**, 1–6.

23 R. L. S. R. Santos, R. Van Eldik and D. De Oliveira Silva, *Inorg. Chem.*, 2012, **51**, 6615–6625.

24 L. Messori, T. Marzo, R. N. F. Sanches, Hanif-Ur-Rehman, D. De Oliveira Silva and A. Merlino, *Angew. Chemie - Int. Ed.*, 2014, **53**, 6172–6175.

25 P. Legzdins, R. W. Mitchell, G. L. Rempel, J. D. Ruddick and G. Wilkinson, *J. Chem. Soc. A Inorganic, Phys. Theor. Chem.*, 1970, 3322–3326.

26 L. Villalobos, J. E. Barker Paredes, Z. Cao and T. Ren, *Inorg. Chem.*, 2013, **52**, 12545–12552.

27 F. Lupi, T. Marzo, G. D'Adamio, S. Cretella, F. Cardona, L. Messori and A. Goti, *ChemCatChem*, 2017, **9**, 4225–4230.

28 R. L. S. R. Santos, A. Bergamo, G. Sava and D. De Oliveira Silva, *Polyhedron*, 2012, **42**, 175–181.

29 G. Ribeiro, M. Benadiba, A. Colquhoun and D. de Oliveira Silva, *Polyhedron*, 2008, **27**, 1131–1137.

30 S. Daniele, S. Taliani, E. Da Pozzo, C. Giacomelli, B. Costa, M. L. Trincavelli, L. Rossi, V. La Pietra, E. Barresi, A. Carotenuto, A. Limatola, A. Lamberti, L. Marinelli, E. Novellino, F. Da Settimo and C. Martini, *Sci. Rep.*, *Sci. Rep.*, **4**, 4749.

31 A. R. Chakravarty and F. A. Cotton, *Inorganica Chim. Acta*, 1985, **105**, 19–29.

32 T. Marzo, A. Pratesi, D. Cirri, S. Pillozzi, G. Petroni, A. Guerri, A. Arcangeli, L. Messori and C. Gabbiani, *Inorganica Chim. Acta*, 2018, **470**, 318–324.

33 S. Daniele, E. Barresi, E. Zappelli, L. Marinelli, E. Novellino, F. Da Settimo, S. Taliani, M. L. Trincavelli and C. Martini, *Oncotarget*, 2016, **7**, 7866–7884.

34 S. Daniele, D. Pietrobono, B. Costa, M. Giustiniano, V. La Pietra, C. Giacomelli, G. La Regina, R. Silvestri, S. Taliani, M. L. Trincavelli, F. Da Settimo, E. Novellino, C. Martini and L. Marinelli, *ACS Chem. Neurosci.*, 2018, **9**, 85–99.

35 A. D. Becke, *J. Chem. Phys.*, 1993, **98**, 5648–5652.

36 P. J. Stephens, F. J. Devlin, C. F. Chabalowski and M. J. Frisch, *J. Phys. Chem.*, 1994, **98**, 11623–11627.

37 I. Tolbatov, C. Coletti, A. Marrone and N. Re, *Inorg. Chem.*, 2020, **59**, 3312–3320.

38 S. Todisco, M. Latronico, V. Gallo, N. Re, A. Marrone, I. Tolbatov and P. Mastrorilli, *Dalt. Trans.*, 2020, **49**, 6776–6789.

39 R. Paciotti, I. Tolbatov, V. Graziani, A. Marrone, N. Re and C. Coletti, in *AIP Conference Proceedings*, American Institute of Physics Inc., 2018, vol. 2040, p. 020019.

40 A. D. Bochevarov, E. Harder, T. F. Hughes, J. R. Greenwood, D. A. Braden, D. M. Philipp, D. Rinaldo, M. D. Halls, J. Zhang and R. A. Friesner, *Int. J. Quantum Chem.*, 2013, **113**, 2110–2142.

41 P. J. Hay and W. R. Wadt, *J. Chem. Phys.*, 1985, **82**, 299–310.

42 D. J. Tannor, B. Marten, R. Murphy, R. A. Friesner, D. Sitkoff, A. Nicholls, B. Honig, M. Ringnald and W. A. Goddard, *J. Am. Chem. Soc.*, 1994, **116**, 11875–11882.

43 I. Tolbatov, N. Re, C. Coletti and A. Marrone, *Inorg. Chem.*, 2020, **59**, 790–800.

44 I. Tolbatov, N. Re, C. Coletti and A. Marrone, *Inorg. Chem.*, 2019, **58**, 11091–11099.

45 R. B. Murphy, D. M. Philipp and R. A. Friesner, *J. Comput. Chem.*, 2000, **21**, 1442–1457.

46 G. A. Kaminski, R. A. Friesner, J. Tirado-Rives and W. L. Jorgensen, *J. Phys. Chem. B*, 2001, **105**, 6474–6487.

47 Infrared and Raman Spectra of Inorganic and Coordination Compounds, Part B: Applications in Coordination, Organometallic, and Bioinorganic Chemistry, 6th Edition | Wiley, https://www.wiley.com/en-us/Infrared+and+Raman+Spectra+of+Inorganic+and+Coordination+Compounds%2C+Part+B%3A+Applications+in+Coordination%2C+Organometallic%2C+and+Bioinorganic+Chemistry%2C+6th+Edition-p-9780471744931, (accessed 15 July 2020).

48 J. M. Antosiewicz and D. Shugar, *Biophys. Rev.*, 2016, **8**, 163–177.

49 P. Delgado-Martínez, A. Elvira-Bravo, R. González-Prieto, J. Priego, R. Jimenez-Aparicio and M. Torres, *Inorganics*, 2014, **2**, 524–536.

50 C. Martín-Santos, E. Michelucci, T. Marzo, L. Messori, P. Szumlas, P. J. Bednarski, R. Mas-Ballesté, C. Navarro-Ranninger, S. Cabrera and J. Alemán, *J. Inorg. Biochem.*, 2015, **153**, 339–345.51 A. Pratesi, D. Cirri, L. Ciofi and L. Messori, *Inorg. Chem.*, 2018, **57**, 10507–10510.

52 L. Massai, A. Pratesi, J. Gailer, T. Marzo and L. Messori, *Inorganica Chim. Acta*, 2019, **495**, 118983.

53 A. Pratesi, D. Cirri, M. D. Đurović, S. Pillozzi, G. Petroni, Ž. D. Bugarčić and L. Messori, *BioMetals*, 2016, **29**, 905–911.

54 T. Togano, M. Mukaida and T. Nomura, *Bull. Chem. Soc. Jpn.*, 1980, **53**, 2085–2086.

55 J. E. Earley, R. N. Bose and B. H. Berrie, *Inorg. Chem.*, 1983, **22**, 1836–1839.

56 A. O. Oyetunji, O. Olubuyide, J. F. Ojo and J. E. Earley, *Polyhedron*, 1991, **10**, 829–835.

57 Hanif-Ur-Rehman, T. E. Freitas, R. N. Gomes, A. Colquhoun and D. de Oliveira Silva, *J. Inorg. Biochem.*, 2016, **165**, 181–191.